Available online at www.sciencedirect.com

ScienceDirect

Procedia CIRP 82 (2019) 113–118

www.elsevier.com/locate/procedia

17th CIRP Conference on Modelling of Machining Operations

Influence of anisotropy of additively manufactured AlSi10Mg parts on chip formation during orthogonal cutting

Eric Segebade[a,*], Michael Gerstenmeyer[a], Stefan Dietrich[b], Frederik Zanger[a], Volker Schulze[a,b]

[a]*wbk Institute of Production Science, Karlsruhe Institute of Technology (KIT), Kaiserstr. 12, 76131 Karlsruhe, Germany*
[b]*Institute for Applied Materials (IAM-WK), Karlsruhe Institute of Technology (KIT), Kaiserstr. 12, 76131 Karlsruhe,Germany*

* Corresponding author. Tel.: +49-721-608-42455 ; fax: +49-721-608-45004. *E-mail address:* eric.segebade@kit.edu

Abstract

Anisotropic behavior of metals can influence manufacturing processes including acting thermo-mechanical loads and resulting surface layer states. In additive manufacturing, the build-up direction influences material states like microstructure, density distribution and stress fields, possibly leading to anisotropic behavior.
In this work, additively manufactured AlSi10Mg is characterized in tension tests in order to determine the anisotropic material deformation behavior due to the build-up procedure. This was implemented in 2D cutting simulations using finite element method. Additionally, orthogonal cutting experiments were performed in order to determine process forces and chip formation, which finally were used in order to validate simulations.

Peer-review under responsibility of the scientific committee of The 17th CIRP Conference on Modelling of Machining Operations

Keywords: Cutting, Anisotropy, Finite-element-method (FEM)

1. Introduction

The use of additive manufacturing (AM) is constantly increasing. In this context, the post treatments also gain importance, especially due to their interaction with the AM-induced material properties, especially, if no subsequent heat treatment is required. In the case of AlSi10Mg, additively manufactured specimen can reach ultimate tensile strengths above those achieved in sand cast specimen, even without heat treatment as Kempen et al. [1] reported. Anisotropic behavior has been reported for AM-materials. Specifically, Tang et al. [2] analyzed the ductility and fracture behavior depending on build-up direction. They found, that “standing” samples exhibit lower flow stress than “lying” specimen. Additionally, the standing samples showed a lower ductility, as interlayer porosity enhanced fracture initiation. Conflicting with this, Zaretsky et al. [3] reported processing orientation independent impact fracture behavior. In general, the tensile failure of AM-AlSi10Mg is reported to be governed by brittle fracture behavior reducing the ductility limit. The AM material reaches roughly 60 % of the fatigue strength of wrought and machined material, as demonstrated by Mower et al. [4]. Obviously, considering the manufacturing induced anisotropy in following process steps should be beneficial, if process parameters or surface integrity features can be optimized.

In this work, the anisotropy effect of AM-AlSi10Mg is characterized in tension tests and subsequently modelled in cutting simulations. Orthogonal cutting experiments are conducted to validate the simulations using cutting forces and chip geometries concerning their thickness as well as the distance of shear bands.

2212-8271
Peer-review under responsibility of the scientific committee of The 17th CIRP Conference on Modelling of Machining Operations
10.1016/j.procir.2019.04.043

2. Experiments

2.1. Additive manufacturing of the specimen

Two types of specimen were manufactured on a SLM 280 HL machine using the parameters in Table 1. One set consisting of differently oriented flat tension specimen was used for tensile tests with a cross section of 7·9 mm² in the measuring range. This assured that processing was identical for all specimen. The other set of differently oriented flat 80·4·20 mm³ specimen was used for orthogonal cutting experiments. Build-up direction was varied as per Figure 1. In the following, the specimen types will be differentiated as "0°", "45°" and "90°". AlSi10Mg powder with a grainsize distribution as shown in Table 2 produced by "m4p material solutions" was used to manufacture all specimen. The specimen exhibited a porosity of ≤ 1%.

Table 1: AM-parameters for specimen manufacture.

Parameter	Contour	Volume	Surface
Hatch		150 µm	
Layer thickness		50 µm	
Power	300 W	250 W	350 W
Speed	600 mm·s^{-1}	555 mm·s^{-1}	800 mm·s^{-1}
Focus	0 mm	-4 mm	-4 mm

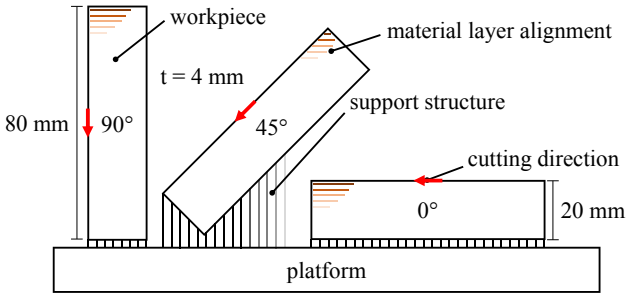

Figure 1: Build-up direction-variants for all specimen sets.

Table 2: Size distribution of powder used for specimen manufacture.

D10	D50	D90
21.2 µm	34.7 µm	57.2 µm

2.2. Characterization of anisotropy

The anisotropy of the AM-samples was analyzed as per DIN EN ISO 6892-1 in quasi-static tensile experiments using multiple strain gauges as well as force measurements. The samples were not subjected to any kind of post treatment apart from wire EDM to reach the end geometry with sufficient accuracy.

2.3. Orthogonal cutting experiments

Orthogonal cutting experiments with the AM-AlSi10Mg specimen were carried out on a Karl Klink vertical broaching machine with a maximum velocity of 200 m·min^{-1}. Before the experiments the specimen were precut with a depth of cut of 0.1 mm in order to remove the EDM-affected layer. The depth of cut applied to the height of 20 mm. While the workpiece is moved vertically, the tool is fixed on a three component dynamometer Type Z 3393 by Kistler. Uncoated cemented carbide cutting tools (type SEHT1204AFN) were used for the experiments. The initial average cutting edge radius was r_β = 8±2 µm, measured tactile using a Mahr perthometer. The tool geometry results in an effective rake angle of 15° and an effective clearance angle of 15°. All experiments were repeated three times and conducted in an overall random order. Process parameters are listed in Table 3. Result comparison was done using specific process forces, which are defined as the measured force divided by the area of uncut material (uncut chip thickness by specimen thickness). Cutting force is measured in the direction of cut, and passive force is measured in the direction of depth of cut.

The chips were subsequently analyzed with regard to shear band distance and thickness using an optical microscope by Zeiss.

Table 3: Orthogonal cutting experiments using the AM-AlSi10Mg specimen.

set no.	cutting velocity v_c in m·min^{-1}	uncut chip thickness h in µm			
1	50	50	100	200	300
2	100	50	100	200	300
3	150	50	100	200	300

3. FE-Simulations

3.1. Flow-stress and anisotropy modelling

A Johnson-Cook material model including energy based exponential failure evolution [5] with basic parameters from Clausen et al. [6] was used to calculate flow stress as function of strain, strain rate and temperature in the finite element (FE) simulations. The parameters used for the Johnson-Cook damage evolution model were adapted from Ijaz et al. [7] and [6]. It has to be noted, that [7] originally concerns AA2024, and [6] AA5083-H116. The parameters used are shown in Table 4. While only one parameter from [6] was modified, the damage model parameters used are very different from the respective start values taken from [7]. Fracture energy was assumed as 27 kJ/m². Further material parameters taken from the Simufact material database and used in the simulations are shown in Table 5. The software used for FE-simulation features an implementation of the Hill 1948 anisotropy [8], which is why this description was used in this work. The model is described in detail and compared to numerous different models by Habraken [9]. As reference, one set of simulations was conducted without the Hill 1948 model activated.

Table 4: Johnson-Cook material model parameters.

Flow stress Parameter	[6] (* = mod.) Value	Failure Parameter	Value
A	167 MPa	D1	0.0
B	396 MPa*	D2	0.873
C	0.001	D3	-0.449
$\dot{\varepsilon}_0$	1 s^{-1}	D4	0.00147
m	0.859	D5	0.8
n	0.551	G_f	27 kJ·m²

Table 5: Material database parameters used in the simulations.

$\lambda_{(T)}$	76 to 188 $W \cdot m^{-1} \cdot K^{-1}$
$C_{p(T)}$	877 to 1546 $J \cdot kg^{-1} \cdot K^{-1}$
$E_{(T)}$	72 to 35 GPa
ν	0.33
ρ	2700 $kg \cdot m^{-3}$
$\alpha_{(T)}$	2 to 2.1·10^{-5} K^{-1}

3.2. Model setup

The model setup in Simufact Forming 15 was similar to that used in a previous work [10]. The model setup is shown in Figure 2. The cutting speed was applied to the workpiece using a combination of a rigid and a heat conducting elastic body, with the heat conducting, rigid cutting tool fixed in space. The heights of the workpieces were defined as 0.4 mm+*h*, leading to similar conditions beneath the cutting tool for all uncut chip thicknesses *h*. The elastic body was modified accordingly. The workpiece mesh is defined using local refinement with a base element edge length of 32 µm. After a convergence study with decreasing minimum element edge lengths, a minimum element edge length of 4 µm was chosen. Continuous remeshing based on element distortion is defined.

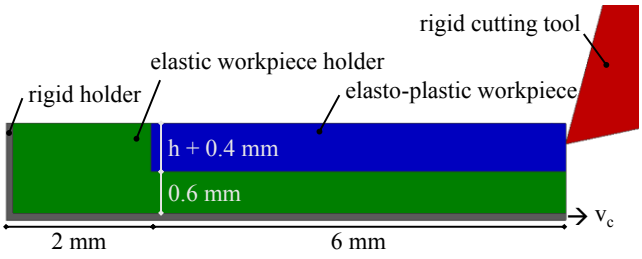

Figure 2: general simulation model setup.

Using a lowered heat capacity for the cutting tool, analogous to that published by Lorentzon et al. [11], ensured thermal steady state conditions. A room temperature boundary condition was set up in 8 mm distance to the edge radius. However, it has to be noted that in cutting of material featuring shear banding behavior, a real steady state does not exist. A relatively high combined friction was assumed on account of the dry condition of the experiments combined with uncoated cutting tools ($\mu = 0.3$, $m = 0.8$).

4. Results and discussion

4.1. Anisotropy

The tensile stresses are shown in Figure 3. The dependency of ultimate tensile strain on build-up direction corresponds to findings published by Tang et al. [2]. The 0° samples reach a maximum strain of nearly 6%, the 45° sample lasting until 3.5%, and the 90° sample at 3%. The measured tensile stresses are virtually independent of build-up direction. The fraction limits differ, with 45° and 90° reaching similar strains, while the 0° specimen exhibits a higher strain limit.

Table 6 lists the anisotropy parameters calculated from width strain and thickness strain for the Hill 1948 model. It has

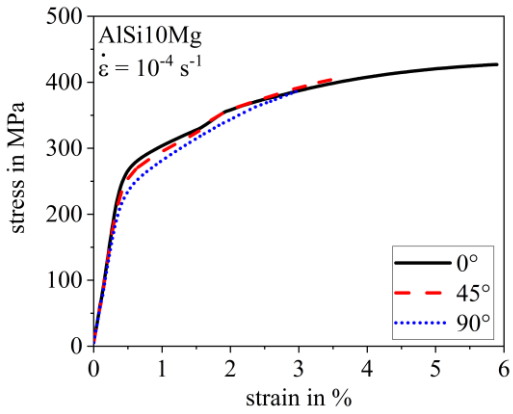

Figure 3: Experimental stress-strain curves from tensile tests dependent on build-up direction.

to be noted, that the Hill model is usually applied to sheet metal forming problems. Modelling the anisotropy using this model results in an assumed, homogenic anisotropy rather than microstructure dependent yield strength. The additively manufactured layers thus could not be considered in this work.

Table 6: Calculated, experimental anisotropy parameters.

$r_{0°}$	$r_{45°}$	$r_{90°}$
1.3405	0.4656	0.9360
$y_{0°}$	$y_{45°}$	$y_{90°}$
278 MPa	247 MPa	231 MPa

4.2. Cutting experiments

The measured specific cutting forces for all experiments are shown in Figure 4 a), and the specific passive forces in Figure 4 b). As expected, the specific forces decrease with increasing uncut chip thickness. It is interesting to note, that the 45° specimen features slightly higher specific cutting forces and slightly lower specific passive forces than the 0° and 90° specimen. The existence of layers of different material properties parallel (0°) and orthogonal (90°) to the cutting direction thus behaves similar regarding the process forces. This also concerns the primary shear zone, which is aligned differently to the layer structure of the specimen, resulting in slight differences in material resistance to deformation. In general, measured cutting forces were very similar only differing a maximum of 21% between 0° and 90° at $v_c = 150$ $m \cdot min^{-1}$ and $h = 100$ µm considering standard deviation.

Figure 5 a) shows the experimental chip ratio r, which is defined as uncut chip thickness divided by chip thickness. Figure 5 b) shows the experimental shear band frequency f_s, which was calculated using the nominal cutting speed divided by the mean distance of shear bands. It is therefore not the shear banding frequency regarding the true chip flow speed.

As can be seen in Figure 5 a), cutting a 45° specimen results in higher chip ratios than cutting the 0° or 90° specimen. This means, that a thinner chip is produced. This, again, can be explained by the material layers, which are parallel (0°) or orthogonal (90°) to the cutting direction. In both cases, a more

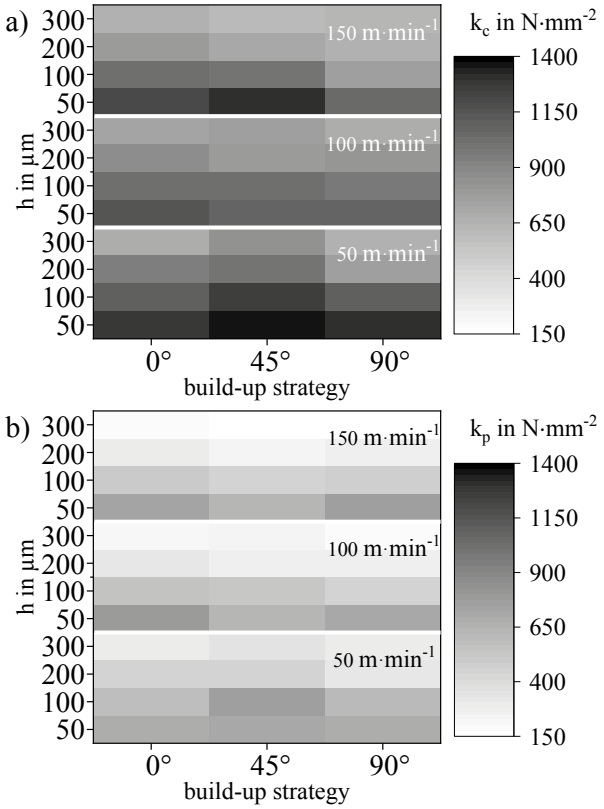

Figure 4: Experimental forces: a) specific cutting forces, b) specific passive forces by uncut chip thickness h, cutting speed and build-up strategy.

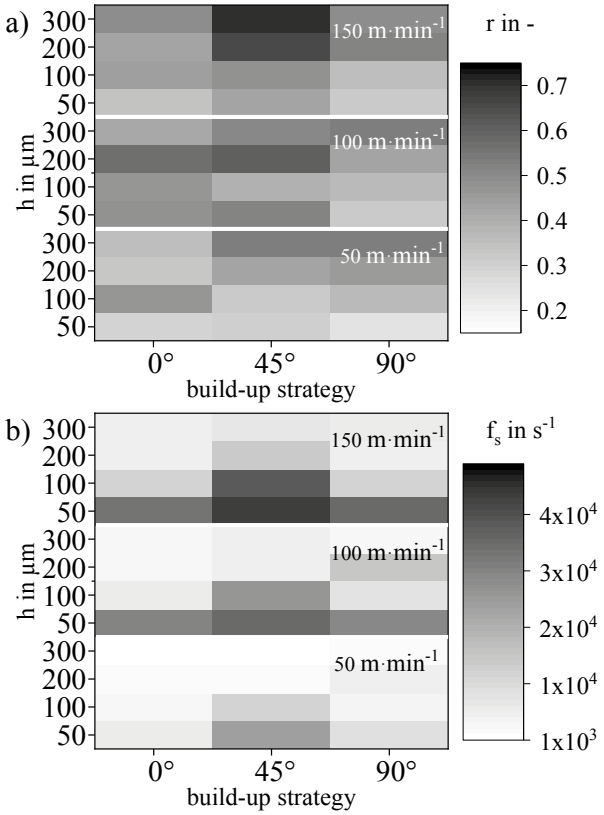

Figure 5: a) Experimental chip ratio r and b) shear-band frequency fs by uncut chip thickness h, cutting speed and build-up strategy.

pronounced shear banding takes place, resulting in overall thicker chips. On the one hand, a parallel layer structure promotes shearing along the layers (0°). On the other hand, an orthogonal structure promotes compression of layers (90°). In both cases, the layers are arranged in an similarily inclined angle regarding the primary shear zone, which changes with cutting depth and speed. Even though the resulting r values for 0° and 90° are similar, the 90° specimen resulted in chips with a more rugged surface. In the 45° specimen the orientation of the layers to the primary shear zone is either closer to a parallel, or orthogonal arrangement. Following the argument of either shearing along layers, or compressing layers, this could lead to an accelerated chip segment formation on account of less resistance along the shear bands. The results shown in Figure 5 b) agree with this hypotheses, clearly showing higher frequencies of chip segments in the 45° specimen. As can be expected, chip segment frequency is generally lower at low speeds, and decreases with chip thickness.

4.3. Cutting simulations

An example of the results including the mesh is shown in Figure 6 for v_c = 50 m·min^{-1} and h = 50 µm at 5 mm length of cut in all variants (isotropic: a), 0°: b), 45°: c) , 90°: d)). The figure also shows the corresponding chips from the experiments. In most instances, the detail of the geometry is lost at a distance from the cutting zone (e.g. in Figure 6 b) and c)). In general the chip morphology is similar between the variants. The curling of the chip and the chip segmentation are most severe for the 90° variant, as could be expected from the experiments. The 45° variant only exhibits a slight curling, again agreeing with the experimental results. Shear banding in the simulations rarely occurred through all of the chip, generally being confined to the surface. Even though the microstructure was not considered in the simulations, the tendency of chip curling was depicted correctly. In general, simulations were more accurate for small uncut chip thicknesses (50 and 100 µm). This may be due to the fact, that

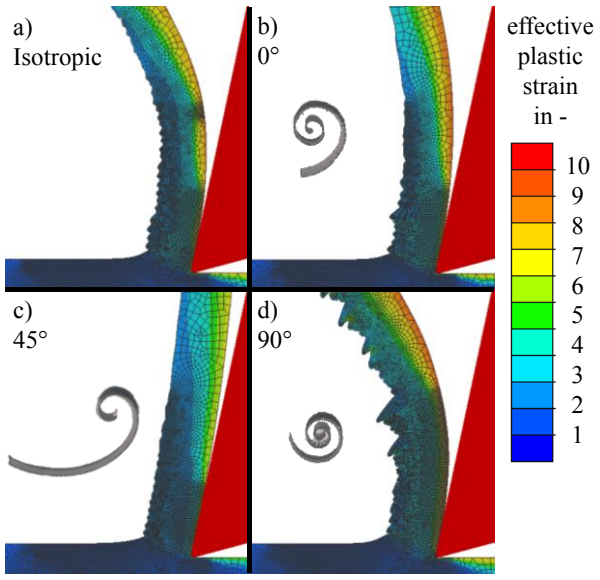

Figure 6: exemplary simulation results of v_c = 50 m·min^{-1} and h = 50 µm: a) isotropic material, b): 0°, c) 45°, d): 90°.

the large chip thicknesses may require an even longer simulated length of cut. Additionally, the damage model was calibrated using 50 µm uncut chip thickness in order to minimize computation times.

Figure 7 shows the comparison of experimental and simulation results. Figure 7 a) concerns the specific cutting force, Figure 7 b) shows the chip ratio, and Figure 7 c) depicts the shear band frequency. The specific passive forces of the simulations were much lower than the experimental ones, which may be due to the contact and friction conditions chosen in the simulations not being based on detailed investigations, including sticking of material to the tool.

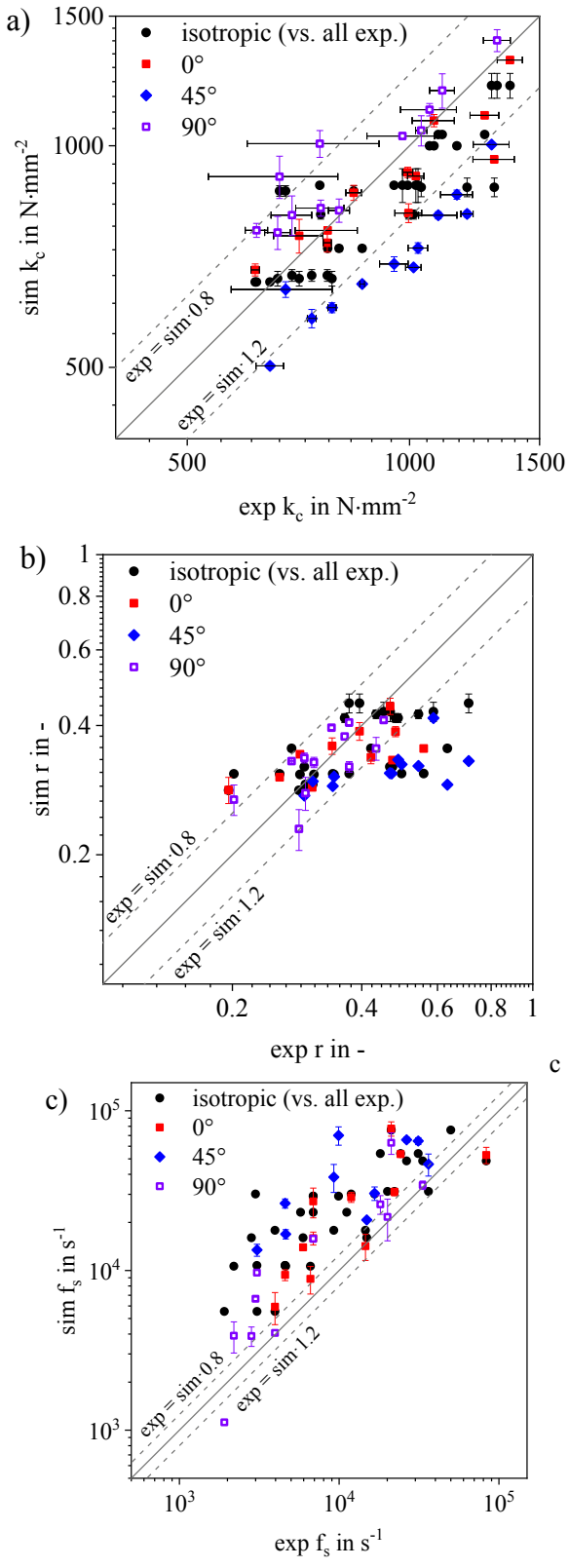

Figure 7: Comparison of simulated and experimental results of a) specific cutting force k_c, b) chip ratio r, and c) shear banding frequency f_s.

The specific cutting force shown in Figure 7 a) is within a 20% error corridor for most experiments, when anisotropy is ignored. Introducing the Hill model slightly changes the spread, with the three variants clearly distinguishable. While the 0° variant remains firmly within the 20% error corridor, the cutting force is underestimated by a little more than 20% for the 45° variant, and slightly overestimated for the 90° variant.

Considering the chip ratio shown in Figure 7 b), most simulations agree with the experimental results. Unsurprisingly, the chip ratio of the 45° variant deviates the most, with the simulations mostly predicting thicker chips. In nearly all instances, the simulations overestimate the shear band frequency (Figure 7 c)). This may well be due to the fact, that indeed the shearing did not take place across the whole width of the chip in the experiments. Furthermore, sub-shears as can be seen in Figure 8 a) were disregarded for the analyses (shown exemplarily for v_c = 100 m·min^{-1}, h = 200 µm with 90° build-up direction). The simulations by contrast are usually easier to analyze because of their 2D-nature, as becomes apparent looking at the analysis in Figure 8 b), showing the corresponding simulation.

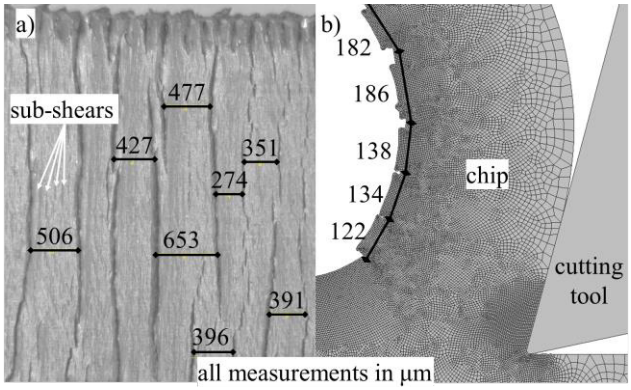

Figure 8: exemplary excerpt of chip analysis: v_c = 100 m·min^{-1}, h = 200 µm with 90° build-up direction: a) experiment b): simulation.

It is interesting to note, that usage of an anisotropic material behavior in the simulations does not yield an increase in simulation accuracy in this instance. This suggests that the parameters of the damage model may need to be adapted for the different build strategies. Additionally, the yield stress model parameters used were not originally fit for AlSi10Mg.

5. Conclusion and outlook

In this work, AlSi10Mg specimen were produced by selective laser melting and subsequently analysed with regard to the resulting anisotropy. Cutting experiments were then conducted to point out differences in specific forces and chip geometry. The direction of cut compared to the layer direction was found to mostly influence the chip geometry and chip segmentation behavior. The largest effect of anisotropy was evident in 45° specimen. This is probably due to the resulting

microstructures alignment to the cutting direction.

The anisotropy model Hill 1948 was fit and implemented in 2D cutting simulations. Even though the Hill model used is one of the simplest models, correct tendencies of chip geometry and chip segmentation behavior could be demonstrated in the simulations. Still, on account of the small effect of anisotropy in this instance, calculations considering the anisotropy were not significantly more accurate than those disregarding anisotropy.

Further work has to first calibrate the material and damage model more sophistically. Afterwards, different implementations of anisotropy need to be compared. For instance, material model and/or damage model parameters could be used depending on build-up direction. Additionally, different anisotropy models need to be investigated. While the best case only requires one of the above, a combination may be more accurate. Last but not least, modelling the microstructure of the material combined with the manufacturing induced stress state may also be one way forward – it needs to be noted however, that depiction of a real microstructure in simulations requires a consistently fine mesh, severely increasing computational times. Analyzing the microstructure of the chips should be part of further investigations regardless.

References

[1] Kempen K, Thijs L, Humbeek V, Kruth JP (2014) Processing AlSi10Mg by selective laser melting: parameter optimisation and material characterisation. In: Materials Science and Technology 31(8): 917-923.

[2] Tang M, Pistorius PC (2017) Anisotropic mechanical behaviour of AlSi10Mg parts produced by slective laser melting. In: Jom 69(3): 516-522.

[3] Zaretsky E, Stern A, Frage N (2017) Dynamic response of AlSi10Mg alloy fabricated by selective laser melting. In: Materials Science & Engineering A 688:364-370.

[4] Mower TM, Long MJ (2016) Mechanical behavior of additive manufactured, powder-bed laser-fused materials. In: Materials Science & Engineering A 651:198-213.

[5] Johnson GR, Cook WH (1985) Fracture characteristics of three metals subjected to various strains, strain rates, temperatures and pressures. In: Engineering Fracture Mechanics 21(1):31-48.

[6] Clausen AH, Børvik T, Hopperstad OS, Benallal A (2003): Flow and fracture characteristics of aluminium alloy AA5038-H116 as function of strain rate, temperature and triaxiality. In: Materials Science and Engineering A364:260-272.

[7] Ijaz H, Zain-ul-abdein M, Saleem W, Asad M, Mabrouki T (2017): Modified Johnson-Cook plasticity model with damage evolution: application to turning simulation of 2XXX aluminium alloy. In: Journal of Mechanics 33(6):777-788.

[8] Hill R (1948) A theory of the yielding and plastic flow of anisotropic metals. In: Proceedings of the Royal Society London A 193:281–297

[9] Habraken AM (2004) Modelling the plastic anisotropy of metals. In Archives of Computational Methods in Engineering, 11(1):3-96.

[10] Segebade E, Kümmel D, Zanger F, Schneider J, Schulze V (2018). Influence of cutting edge asymmetry on grain refinement of TiAl6V4. In: Procedia CIRP 71:232-237.

[11] Lorentzon J, Järvstråt (2008) Modelling tool wear in cemented-carbide machining alloy 718. In: Int. J. Machine Tools & Manufacture 48:1072-1080.